Robust Burn Control in ITER Under Deuterium-Tritium Concentration Variations in the Fueling Lines

A. Pajares and E. Schuster
Lehigh University
Bethlehem, Pennsylvania 18015, USA
Email: andres.pajares@lehigh.edu

Abstract

Tight regulation of the burn condition in ITER has been proven possible in simulations even under time-dependent variations in the fuel concentration by the use of robustification techniques. One of the most fundamental control problems arising in ITER and future burning-plasma tokamaks is the regulation of the plasma temperature and density to produce a determined amount of fusion power while avoiding possible thermal instabilities. Such problem, known as burn control, will require the development of controllers that integrate all the available actuators in the tokamak. Moreover, the complex dynamics of the burning plasma and the uncertain nature of some of its magnitudes suggest that nonlinear, robust burn controllers will be necessary. Available actuators in the burn control problem are auxiliary power modulation, fueling rate modulation, and impurity injection. Also, recent experiments in the DIII-D tokamak have shown that in-vessel coil-current modulation can be used for burn control purposes. The in-vessel coils generate non-axisymmetric magnetic fields that have the capability to decrease the plasma-energy confinement time, which allows for regulating the plasma energy during positive energy perturbations. In this work, in-vessel coil-current modulation is included in the control scheme, and it is used in conjunction with the other previously mentioned actuators to design a nonlinear burn controller which is robust to variations in the deuterium-tritium concentration of the fueling lines. Furthermore, fueling rate modulation is not only used to control the plasma density, but also to control the plasma energy, if necessary, by means of isotopic fuel tailoring. Isotopic fuel tailoring is a particular way of fueling the burning plasma which allows for reducing the fusion power produced and, therefore, also gives the opportunity to decrease the plasma energy when needed. The model-based nonlinear controller is synthesized from a zero-dimensional model of the burning-plasma dynamics. A nonlinear simulation study is used to illustrate the successful controller performance in an ITER-like scenario in which unknown variations of the deuterium-tritium concentration of the fueling lines are emulated.

1. Introduction

Tight regulation of the burn condition in ITER has been proven possible in simulations even under time-dependent variations in the fuel concentration by the use of robustification techniques. In the context of developing the necessary burn controllers for future burning-plasma tokamaks, a robust, nonlinear, model-based controller has been designed and successfully tested in nonlinear simulations. This burn control algorithm integrates the most effective actuators available for burn control, namely auxiliary power modulation, in-vessel coil-current modulation, fueling rate modulation, and controlled impurity injection. The controller makes use of the two pellet injectors available in ITER's initial phase: a Deuterium (D) injector (with pellets of 100% D nominal concentration) and a Deuterium-Tritium (D-T) injector (with pellets of 10%D-90%T nominal concentration). The D-T concentration in these fueling lines may vary over time and the estimation of such variation during operation may be difficult or not even possible. The developed burn controller has been designed to be robust to unknown variations in the D-T concentrations of the fueling lines over time such as biases and drifts, and shows a satisfactory performance in nonlinear simulations for different ITER-like scenarios.

The control algorithm considers that the primary methods to regulate the plasma energy are auxiliary power modulation and in-vessel coil-current modulation. The inclusion of in-vessel coil-current modulation as an actuator is motivated by recent experiments in the DIII-D tokamak [1]. The non-axisymmetric magnetic fields generated by the in-vessel coils have the capability to decrease the plasma-energy confinement time, which allows for regulation of the plasma energy. Fueling rate modulation is used in isotopic fueling mode to control the plasma energy and total density if both the auxiliary power and the in-vessel coil current saturate, or if the total plasma density, n, is such that $n > 2f_{GW}n_{GW}$, where $0 < f_{GW} \leq 1$ is a design parameter, and n_{GW} is the Greenwald density limit. Otherwise, fueling rate modulation is exclusively used to control the D and T densities. Reduction of the plasma energy by in-vessel coil-current modulation, instead of by isotopic fueling, allows for smaller control actions and finer plasma-energy regulation, provided that a careful controller design is followed. Impurity injection is kept as a backup actuator to decrease the plasma energy provided that $n \leq 2f_{GW}n_{GW}$. All these actuation methods are integrated within one single burn-control algorithm that operates them simultaneously and makes decisions about which one is the most suitable to ensure successful regulation of the burn condition. The robust, nonlinear, feedback controller has been tested in closed-loop simulations for different ITER-like scenarios. Moreover, its performance has been compared to the performances of both a nominal nonlinear feedback controller that is not robust against variations in the D-T concentrations of the fueling lines and a feedforward control law designed based on the nominal model (not capturing possible variations in the D-T fuel concentrations).

2. Burning Plasma Model

The model utilized in this work is a zero-dimensional model in which all variables can be considered as volume-averaged magnitudes. It takes into account the existence of the different types of particles that compose the burning plasma: D, T, α particles, and impurities. Approximate particle density and energy balance equations are employed to characterize the dynamics of the burning plasma.
The balance equations for the D and T densities, n_D and n_T, are given by

$$\frac{dn_D}{dt} = -\frac{n_D}{\tau_D} + S_D^{inj} - S_\alpha, \quad \frac{dn_T}{dt} = -\frac{n_T}{\tau_T} + S_T^{inj} - S_\alpha, \tag{1}$$

where t is the time, the terms $-n_D/\tau_D$ and $-n_T/\tau_T$ represent the transport of D and T particles out of the plasma core, respectively, τ_D and τ_T are the D and T confinement times, respectively, S_D^{inj} and S_T^{inj} are the controllable D and T injection rates, respectively, and S_α is the source of α particles arising from nuclear fusion reactions,

$$S_\alpha = n_D n_T \langle\sigma v\rangle = \gamma(1-\gamma)(n_D + n_T)^2 \langle\sigma v\rangle, \tag{2}$$

where γ is the tritium fraction, defined as $\gamma = n_T/(n_D + n_T)$, and $\langle\sigma v\rangle$ is the cross section of the D-T reaction, which is modeled as $\langle\sigma v\rangle = \exp(a_1/T^r + a_2 + a_3 T + a_4 T^2 + a_5 T^3 + a_6 T^4)$, where a_i and r are constant scaling parameters [2], and T is the plasma temperature (it is assumed that ion and electron temperatures are the same, $T \triangleq T_e = T_i$). Modeling of wall recycling effects is omitted in this work to simplify the exposition due to space constraints but it is included in [3]. The balance equation for the α-particle density, n_α, is given by

$$\frac{dn_\alpha}{dt} = -\frac{n_\alpha}{\tau_\alpha} + S_\alpha, \tag{3}$$

where the term $-n_\alpha/\tau_\alpha$ represents the transport of α particles out of the plasma core, and τ_α is the confinement time of the α particles. For simplicity, only one type of impurity particle is considered in this work, although a more complex model could be used. The time evolution of the impurity particle density, n_I, is given by

$$\frac{dn_I}{dt} = -\frac{n_I}{\tau_I} + S_I^{sp} + S_I^{inj}, \tag{4}$$

where the term $-n_I/\tau_I$ represents the transport of impurities out the plasma core, τ_I is the confinement time of the corresponding impurity particle, S_I^{inj} is the source of impurities injected for control purposes, and S_I^{sp} is the source of impurities arising from sputtering, which is modeled as

$$S_I^{sp} = f_I^{sp}\left(\frac{n}{\tau_I} + \frac{dn}{dt}\right), \tag{5}$$

where $f_I^{sp} > 0$ is a constant parameter, and n is the total plasma density,

$$n = n_i + n_e = 3n_\alpha + 2n_D + 2n_T + (1 + Z_I)n_I, \tag{6}$$

where $n_i = n_\alpha + n_D + n_T + n_I$ is the ion density, and n_e is the electron density, which is related to the density of the ions by the quasi-neutrality condition, $n_e = 2n_\alpha + n_D + n_T + Z_I n_I$, where Z_I is the atomic number of the impurities. The plasma energy, E, is related to n and T by

$$E = \frac{3}{2}(n_i T_i + n_e T_e) = \frac{3}{2} nT, \tag{7}$$

where the assumption $T \triangleq T_e = T_i$ has been used. The energy density balance in the plasma is given by

$$\frac{dE}{dt} = -\frac{E}{\tau_E} + P \triangleq -\frac{E}{\tau_E} + P_\alpha + P_{Ohm} - P_{rad} + P_{aux}, \tag{8}$$

where τ_E is the energy confinement time, $P \triangleq P_\alpha + P_{Ohm} - P_{rad} + P_{aux}$ is the total power density, P_α is the α-particle heating power density, P_{Ohm} is the ohmic heating power density, P_{rad} is the radiative power density, and P_{aux} is the auxiliary power density injected into the plasma. The α-particle power is given by $P_\alpha = Q_\alpha S_\alpha$, where $Q_\alpha = 3.52$ MeV. The ohmic power is given by $P_{Ohm} = 2.8\times10^{-9}(Z_{eff} I_p^2)/(a^4 T^{3/2})$, where $Z_{eff} = (4n_\alpha + n_D + n_T + Z_I^2 n_I)/n_e$ is the effective atomic number of the plasma ions, I_p is the plasma current, a is the minor radius of the tokamak, and T has to be given in keV. The radiative power is composed by three terms, $P_{rad} = P_{brem} + P_{line} + P_{rec}$, where P_{brem} is the Bremsstrahlung term, P_{line} is the line radiation term, and P_{rec} is the recombination term. Each term is given by $P_{brem} = 4.8\times10^{-37}(\sum_j n_j Z_j^2) n_e \sqrt{T}$, $P_{line} = 1.8\times10^{-38}(\sum_j n_j Z_j^4) n_e T^{-1/2}$, and $P_{rec} = 4.1\times10^{-40}(\sum_j n_j Z_j^6) n_e T^{-3/2}$, where the summation in j is done for all types of ions in the plasma, and T has to be given in keV [4]. The ITER's parameters used in this work are $I_p = 15$ MA, $R = 6.2$ m, $a = 2.0$ m, $B_T = 5.3$ T, $\kappa_{95} = 1.7$, and $V = 837$ m^3.

2.1. Effect of In-vessel Coil Currents on Energy Confinement Time

For τ_E, the IPB98(y,2) scaling is used [5],

$$\tau_E = 0.0562 H_H I_p^{0.93} B_T^{0.15} n_{\mathrm{e19}}^{0.41} M^{0.19} R^{1.97} \epsilon^{0.58} \kappa_{95}^{0.78} (PV)^{-0.69}, \tag{9}$$

where H_H is the so-called H-factor, I_p is the plasma current in MA, B_T is the toroidal magnetic field, $n_{\mathrm{e},19}$ is the electron density in 10^{19} m^{-3}, M is the plasma effective mass in amu, R is the major radius, $\epsilon = a/R$ is the inverse aspect ratio, where a is the minor radius, κ_{95} is the elongation at the 95 % flux surface/separatrix, P is the total power density in MW m^{-3}, and V is the plasma volume. It is assumed that all particle confinement times scale with τ_E, i.e., $\tau_\alpha = k_\alpha \tau_E$, $\tau_D = k_D \tau_E$, $\tau_T = k_T \tau_E$, $\tau_I = k_I \tau_E$, where k_α, k_D, k_T and k_I are constant parameters.
The H-factor, H_H, is a scalar which represents the uncertainty of the IPB98(y,2) scaling under different scenarios and operating conditions. A value of $H_H = 1$ yields the best fit to experimental data in the international database. It can also be seen as a measurement of the plasma confinement quality which comprises effects not explicitly included in the IPB98(y,2) scaling. Amongst those effects, perturbations in the tokamak magnetic configuration can be considered. In particular, those magnetic perturbations introduced by the non-axisymmetric magnetic fields generated by the in-vessel coils have a proven impact on H_H in DIII-D plasmas with relatively low collisionality ν_e and relatively low n_e ($\nu_e \approx 0.1$, $n_e \approx 3.5 \times 10^{19} m^{-3}$) [1]. In these experiments, activation of the in-vessel coils implied a decrease in H_H and, consequently, a decrease in τ_E. Tokamak plasmas with higher ν_e and n_e, on the contrary, did not show H_H variations under application of non-axisymmetric magnetic fields [6]. Using the experimental data available for DIII-D in [1, 6], the following control-oriented scaling is used to account for the influence of the in-vessel-coil current, denoted by I_{coil}, on H_H,

$$H_H = H_{H,0} + \left(\frac{n_e}{n_{e,0}}\right)^{-\delta} \left(\frac{\nu_e}{\nu_{e,0}}\right)^{-\lambda} [C_2 I_{coil}^2 + C_1 I_{coil}], \tag{10}$$

where $H_{H,0}$ is the H-factor without activation of the in-vessel coils, $n_{e,0}$ and $\nu_{e,0}$ are the electron density and collisionality, respectively, corresponding to a nominal working point for which experimental data is available, and $\delta > 0$, $\lambda > 0$, C_1 and C_2 are constants which are determined from the experimental data. Because the in-vessel coils can only reduce H_H, the term $[C_2 I_{coil}^2 + C_1 I_{coil}]$ is always ≤ 0, $\forall I_{coil} \geq 0$.

2.2. Uncertainty Characterization for the D-T Concentration in the Fueling Lines

The fueling rates associated with the two fueling lines available in the initial phase of ITER (D-T pellet injector and D pellet injector) are denoted as $S^{inj}_{DT-line}$ and S^{inj}_{D-line}, respectively, and are considered as directly controllable magnitudes. S^{inj}_D and S^{inj}_T can be expressed, in terms of $S^{inj}_{DT-line}$ and S^{inj}_{D-line}, as

$$S^{inj}_D = (1-\gamma_{DT-line}) S^{inj}_{DT-line} + (1-\gamma_{D-line}) S^{inj}_{D-line}, \qquad S^{inj}_T = \gamma_{DT-line} S^{inj}_{DT-line} + \gamma_{D-line} S^{inj}_{D-line}, \tag{11}$$

where $\gamma_{DT-line} \in [0,1]$ and $\gamma_{D-line} \in [0,1]$ are parameters that characterize the T concentration in the D-T and D pellet injectors, respectively. Therefore, in the nominal case, $\gamma_{DT-line} = \gamma^{nom}_{DT-line} \triangleq 0.9$ and $\gamma_{D-line} = \gamma^{nom}_{D-line} \triangleq 0$. However, as introduced above, unknown variations over time in the D-T concentrations are expected in the fueling lines. Such uncertainties are modeled as $\gamma_{DT-line} = \gamma^{nom}_{DT-line} + \delta_{DT-line}$, $\gamma_{D-line} = \gamma^{nom}_{D-line} + \delta_{D-line}$, where $\delta_{DT-line}$ and δ_{D-line} are the unknown variations in the D-T concentration in the D-T and D pellet injectors, respectively. From its definition, it is found that $\delta_{DT-line} \in [-0.9, 0.1]$ and $\delta_{D-line} \in [0,1]$, so these uncertainties are bounded.

2.3. Total Density and Tritium Fraction Dynamics

Because isotopic fueling controls E by regulating γ, and stability limits exist for n, it is convenient to control n and γ under isotopic fueling mode, instead of n_D and n_T. From (6), the definition of γ, and the balance equations (1), (3), and (4), it is possible to write the balance equations for n and γ, which are given by

$$\begin{aligned} \frac{dn}{dt} &= 3\left[-\frac{n_\alpha}{\tau_\alpha} + S_\alpha\right] + (3n_\alpha + (1+Z_I)\, n_I - n)\left(\frac{1-\gamma}{\tau_D} + \frac{\gamma}{\tau_T}\right) \\ &\quad -4S_\alpha + 2(S^{inj}_{D-line} + S^{inj}_{DT-line}) + (1+Z_I)\left[-\frac{n_I}{\tau_I} + S^{inj}_I + S^{sp}_I\right], \end{aligned} \tag{12}$$

$$\begin{aligned} \frac{d\gamma}{dt} &= \gamma(1-\gamma)\left(\frac{1}{\tau_D} - \frac{1}{\tau_T}\right) + \frac{2}{n - 3n_\alpha - (1+Z_I)\, n_I}\Big\{-S_\alpha + \gamma_{D-line} S^{inj}_{D-line} \\ &\quad + \gamma_{DT-line} S^{inj}_{DT-line} - \gamma\left[-2S_\alpha + S^{inj}_{D-line} + S^{inj}_{DT-line}\right]\Big\}. \end{aligned} \tag{13}$$

As a result, two states, x, are utilized in this work for control design. If fueling rate modulation directly controls n_D and n_T, then $x = [n_\alpha, n_D, n_T, n_I, E]^T$. If isotopic fuel tailoring controls n and γ, then $x = [n_\alpha, n, \gamma, n_I, E]^T$. The inputs to the system are P_{aux}, I_{coil}, S^{inj}_I, S^{inj}_{D-line}, and $S^{inj}_{DT-line}$.

3. Operating Points and Control Objective

The equilibria of the balance equations (1), (3), (4) and (8) (or alternatively, (3), (4), (8), (12) and (13)), which define the operating points of the tokamak, are obtained by forcing the time derivatives to zero. Upper bars are used to denote equilibrium values. It can be noted that $\bar{S}_I^{inj} = 0$ is set, as controlled impurity injection is only utilized as a back-up actuator to decrease E when $E > \bar{E}$. In addition, at any operating point, it is desirable that $\bar{\tau}_E$ is as large as possible, thus $\bar{I}_{coil} = 0$ is imposed. Then, the equilibrium system is composed by 5 equations with 8 unknowns (5 state variables + 3 inputs), so 3 variables must be specified in order to find a unique solution. The variables fixed in this work to solve for the equilibrium, and therefore to define the tokamak operating point, are $T = \bar{T}$, $\gamma = \bar{\gamma}$, and $\beta_N = \bar{\beta}_N$, where $\beta_N = \beta_t a B_T / I_p[\%]$, $\beta_t = 4\mu_0 E/(B_T^2 V)$, where μ_0 is the vacuum permeability.
The dynamic equations for the state error, defined as $\tilde{x} \triangleq x - \bar{x} = [\tilde{n}_\alpha, \tilde{n}_D, \tilde{n}_T, \tilde{n}_I, \tilde{E}]^T$ when isotopic fueling is not employed, are given by

$$\frac{d\tilde{n}_\alpha}{dt} = -\frac{\bar{n}_\alpha}{\tau_\alpha} - \frac{\tilde{n}_\alpha}{\tau_\alpha} + S_\alpha, \tag{14}$$

$$\frac{d\tilde{n}_D}{dt} = -\frac{\bar{n}_D}{\tau_D} - \frac{\tilde{n}_D}{\tau_D} - S_\alpha + S_D^{inj}, \tag{15}$$

$$\frac{d\tilde{n}_T}{dt} = -\frac{\bar{n}_T}{\tau_T} - \frac{\tilde{n}_T}{\tau_T} - S_\alpha + S_T^{inj}, \tag{16}$$

$$\frac{d\tilde{n}_I}{dt} = -\frac{\bar{n}_I}{\tau_I} - \frac{\tilde{n}_I}{\tau_I} + S_I^{inj} + S_I^{sp}, \tag{17}$$

$$\frac{d\tilde{E}}{dt} = -\frac{\bar{E}}{\tau_E} - \frac{\tilde{E}}{\tau_E} + P_\alpha + P_{Ohm} - P_{rad} + P_{aux}. \tag{18}$$

If isotopic fueling is used, then $\tilde{x} \triangleq x - \bar{x} = [\tilde{n}_\alpha, \tilde{n}, \tilde{\gamma}, \tilde{n}_I, \tilde{E}]^T$, and (15) and (16) are substituted by the dynamic equations for the n and γ error variables, denoted by $\tilde{n}$ and $\tilde{\gamma}$, respectively. Details can be found in [3].
The control objective is to drive the state error $\tilde{x}$ to zero, or alternatively, the state x to its equilibrium value $\bar{x}$.

4. Controller Design

4.1. Control Law for the Nominal System ($\delta_{D-line} = 0, \delta_{DT-line} = 0$)

Step 1: Auxiliary Power Modulation. If P_{aux} is set to

$$P_{aux}^{unsat} = \frac{\bar{E}}{\tau_E} - P_\alpha - P_{Ohm} + P_{rad} - K_P \tilde{E}, \tag{19}$$

where $K_P > 0$ is a design parameter, then (18) is reduced to $d\tilde{E}/dt = -(1/\tau_E + K_P)\tilde{E}$, and using a Lyapunov function [7] $V_{\tilde{E}} = \frac{1}{2}\tilde{E}^2 > 0$, yields $\dot{V}_{\tilde{E}} = -(1/\tau_E + K_P)\tilde{E}^2 < 0$. This ensures global asymptotical stability for $\tilde{E}$ (i.e., $\tilde{E} \to 0$). In this case, neither in-vessel coil-current modulation (Step 2) nor impurity injection (Step 5) are used, i.e., $I_{coil} \equiv 0$ and $S_I^{inj} \equiv 0$. Moreover, $\tilde{n}_D$ and $\tilde{n}_T$ are controlled by fueling rate modulation (Step 3) as long as $n \leq 2 f_{GW} n_{GW}$, where $n_{GW} = \frac{I_p}{\pi a^2} 10^{20} m^{-3}$ is the Greenwald density limit (I_p in MA), and $0 < f_{GW} \leq 1$ is a design parameter. Otherwise, $\tilde{n}_D$ and $\tilde{n}_T$ are controlled by isotopic fueling (Step 4). However, it may not be possible to set $P_{\rm aux} = P_{\rm aux}^{\rm unsat}$ because there exist saturation limits, which are denoted as $P_{\rm aux}^{\rm max}$ and $P_{\rm aux}^{\rm min}$. If $P_{\rm aux}^{\rm unsat} > P_{\rm aux}^{\rm max}$, the control algorithm keeps $P_{\rm aux} = P_{\rm aux}^{\rm max}$, but it cannot be ensured that $\tilde{E} \to 0$. The only possible ways to cope with this limitation are either to increase $P_{\rm aux}^{\rm max}$ or to improve the machine parameters ($I_{\rm p}$, $B_{\rm T}$, etc.). On the other hand, if $P_{\rm aux}^{\rm unsat} < P_{\rm aux}^{\rm min}$, the control algorithm keeps $P_{\rm aux} = P_{\rm aux}^{\rm min}$, but it cannot be ensured that $\tilde{E} \to 0$. In that case, the controller is designed to use in-vessel coil-current modulation (Step 2), isotopic fueling (Step 4), and/or impurity injection (Step 5) to regulate $\tilde{E}$.

Step 2: In-vessel Coil-current Modulation. If τ_E is set to

$$\tau_E^{unsat} = \frac{\bar{E}}{P^{min} + K_{\tau_E}\tilde{E}}, \tag{20}$$

where $P^{min} = P_\alpha + P_{Ohm} - P_{rad} + P_{aux}^{min}$, and $K_{\tau_E} > 0$ is a design parameter, then (18) is reduced to $d\tilde{E}/dt = -(1/\tau_E + K_{\tau_E})\tilde{E}$. Using $V_{\tilde{E}} = \frac{1}{2}\tilde{E}^2 > 0$, then $\dot{V}_{\tilde{E}} = -(1/\tau_E + K_{\tau_E})\tilde{E}^2 < 0$, which ensures global asymptotical stability for $\tilde{E}$ (i.e., $\tilde{E} \to 0$). The required value I_{coil}^{unsat} to set τ_E as in (20) is obtained from (9), (10), and (20) by solving the following nonlinear equation,

$$C_2 (I_{coil}^{unsat})^2 + C_1 I_{coil}^{unsat} = \left(\frac{\tau_E^{unsat}}{K_{IPB98(y,2)}} - H_{H,0}\right)\left(\frac{n_e}{n_{e,0}}\right)^\delta \left(\frac{\nu_e}{\nu_{e,0}}\right)^\lambda, \tag{21}$$

where $K_{IPB98(y,2)} = 0.0562 I_p^{0.93} B_T^{0.15} n_{e,19}^{0.41} M^{0.19} R^{1.97} \epsilon^{0.58} \kappa_{95}^{0.78} (P^{min})^{-0.69} V^{-0.69}$. In this case, $\tilde{n}_D$ and $\tilde{n}_T$ are controlled by fueling rate modulation (Step 3), except if $n > 2 f_{GW} n_{GW}$, when again isotopic fueling (Step 4) is activated. However, it may not be possible to set $I_{coil} = I_{coil}^{unsat}$ because there exists saturation limits, i.e., $0 \leq I_{coil} \leq I_{coil}^{max}$. $I_{coil}^{unsat} \leq 0$ is an indication that indeed P_{aux} modulation can regulate $\tilde{E}$ (Step 1) on its own. In this case, in-vessel coil-current modulation is not necessary and the controller makes $I_{coil} \equiv 0$. On the other hand, if $I_{coil}^{unsat} > I_{coil}^{max}$, the controller sets $I_{coil} = I_{coil}^{max}$ and uses isotopic fueling (Step 4) and/or impurity injection (Step 5) to further regulate $\tilde{E}$.

Step 3: Fueling Rate Modulation ($\tilde{n}_D$ and $\tilde{n}_T$ Control). If S_D^{inj} and S_T^{inj} are set to

$$S_D^{inj,unsat} = S_\alpha + \frac{\bar{n}_D}{\tau_D} - K_D \tilde{n}_D, \qquad S_T^{inj,unsat} = S_\alpha + \frac{\bar{n}_T}{\tau_T} - K_T \tilde{n}_T, \tag{22}$$

where $K_D > 0$ and $K_T > 0$ are design parameters, then (15) and (16) are reduced to $d\tilde{n}_D/dt = -(1/\tau_D + K_D)\,\tilde{n}_D$ and $d\tilde{n}_T/dt = -(1/\tau_T + K_T)\,\tilde{n}_T$, respectively. Using $V_{\tilde{n}_{DT}} = \frac{1}{2}(\tilde{n}_D^2 + \tilde{n}_T^2)$, it is found that $\dot{V}_{\tilde{n}_{DT}} = -(1/\tau_D + K_D)\,\tilde{n}_D^2 - (1/\tau_T + K_T)\,\tilde{n}_T^2 < 0$, thus both $\tilde{n}_D$ and $\tilde{n}_T$ evolutions are globally asymptotically stable (i.e., $\tilde{n}_D \to 0$ and $\tilde{n}_T \to 0$). The stabilizing values for S_{D-line}^{inj} and $S_{DT-line}^{inj}$ are obtained from solving (11) together with (22). Nonetheless, as before, it may not be possible to set $S_{D-line}^{inj} = S_{D-line}^{inj,unsat}$ and/or $S_{DT-line}^{inj} = S_{DT-line}^{inj,unsat}$ because there exist physical saturation limits, that are denoted by $S_{D-line}^{inj,max}$, $S_{D-line}^{inj,min}$, $S_{DT-line}^{inj,max}$, and $S_{DT-line}^{inj,min}$. If $S_{D-line}^{inj}/S_{DT-line}^{inj}$ is larger or smaller than its applicable saturation limits, the controller keeps $S_{D-line}^{inj}/S_{DT-line}^{inj}$ at the saturation limit that has been violated, and no further steps in the control algorithm are activated. The asymptotic stability of $\tilde{n}_D$ and/or $\tilde{n}_T$ cannot be ensured unless the controller recovers from the saturation limits. This is not an inherent problem of the control algorithm but just a physical limitation in the actuation capability of the tokamak. Finally, it can be showed that, if $\tilde{E}$, $\tilde{n}_D$, and $\tilde{n}_T$ are driven to zero, then $\tilde{n}_\alpha$ and $\tilde{n}_I$ are also driven to zero as $t \to \infty$ provided that $S_I^{inj} \equiv 0$ [3], so the control objective is achieved.

Step 4: Fueling Rate Modulation ($\hat{\gamma}$ and $\tilde{n}$ Control). By using isotopic fueling, the controller attempts to drive $\gamma \to \gamma^*$ to make $\tilde{E}$ asymptotically stable. This γ^* value is obtained by solving the nonlinear equation

$$\gamma^*(1-\gamma^*) = \frac{\frac{\bar{E}}{\tau_E} - P_{Ohm} - P_{aux} + P_{rad} - K_{\gamma,1}\tilde{E}}{Q_\alpha (n_D + n_T)^2 \langle \sigma v \rangle_{DT}}, \tag{23}$$

where $K_{\gamma,1} > 0$ is a design parameter. In this case, (18) reduces to $d\tilde{E}/dt = -\left(1/\tau_E + K_{\gamma,1}\right)\tilde{E}$, and using the same Lyapunov function $V_{\tilde{E}} = \frac{1}{2}\tilde{E}^2 > 0$ as before, global asymptotical stability of $\tilde{E}$ is ensured because $\dot{V}_{\tilde{E}} = -\left(1/\tau_E + K_{\gamma,1}\right)\tilde{E}^2 < 0$. For stability analysis, it is convenient to define $\hat{\gamma} \triangleq \gamma - \gamma^*$ since making $\hat{\gamma} \to 0$ is equivalent to making $\gamma \to \gamma^*$. Taking S_T^{inj} as

$$S_T^{inj,unsat} = \frac{\gamma[-2S_\alpha + S_D^{inj,unsat}] + S_\alpha + v}{1-\gamma}, \tag{24}$$

and using the definition for $\hat{\gamma}$ and (13), it is possible to write $d\hat{\gamma}/dt = \gamma(1-\gamma)\,(1/\tau_D - 1/\tau_T) + \frac{v}{n_D+n_T}$. By taking $v = -(n_D+n_T)[\gamma(1-\gamma)\frac{1}{\tau_D} + \frac{\gamma^2-\gamma^*}{\tau_T} + K_{\gamma,2}\hat{\gamma}]$, where $K_{\gamma,2} > 0$ is a design parameter, it is found that $d\hat{\gamma}/dt = -\left(1/\tau_T + K_{\gamma,2}\right)\hat{\gamma}$. Then, using $V_{\hat{\gamma}} = \frac{1}{2}\hat{\gamma}^2$, it is found that $\dot{V}_{\hat{\gamma}} = -\left(1/\tau_T + K_{\gamma,2}\right)\hat{\gamma}^2 < 0$. Thus, the $\hat{\gamma}$ evolution is globally asymptotically stable. Taking S_D^{inj} as

$$S_D^{inj,unsat} = \frac{n_D}{\tau_D} + \frac{n_T}{\tau_T} + 2S_\alpha - S_T^{inj,unsat} + w, \tag{25}$$

and using (12), it is possible to write $d\tilde{n}/dt = 3\,(-n_\alpha/\tau_\alpha + S_\alpha) + (1+Z_I)\left(-n_I/\tau_I + S_I^{inj} + S_I^{sp}\right) + 2w$, where $\tilde{n} \triangleq n - \bar{n}$. By taking $w = -\frac{1}{2}\left[3(-n_\alpha/\tau_\alpha + S_\alpha) + (1+Z_I)\left(-n_I/\tau_I + S_I^{inj} + S_I^{sp}\right) + K_n\tilde{n}\right]$, where $K_n > 0$ is a design parameter, it is found that $d\tilde{n}/dt = -K_n\tilde{n}$. Using $V_{\tilde{n}} = \frac{1}{2}\tilde{n}^2$ ensures that the $\tilde{n}$ evolution is globally asymptotically stable because $\dot{V}_{\tilde{n}} = -K_n\tilde{n}^2 < 0$. Solving (24)-(25) for $S_D^{inj,unsat}$ and $S_T^{inj,unsat}$ yields

$$S_D^{inj,unsat} = (1-\gamma)\left(\frac{n_D}{\tau_D} + \frac{n_T}{\tau_T} + w\right) + S_\alpha - v, \quad S_T^{inj,unsat} = \gamma\left(\frac{n_D}{\tau_D} + \frac{n_T}{\tau_T} + w\right) + S_\alpha + v. \tag{26}$$

The stabilizing values for S_{D-line}^{inj} and $S_{DT-line}^{inj}$ are obtained from solving (11) together with (26). If the saturation limits $S_{D-line}^{inj,max}$, $S_{D-line}^{inj,min}$, $S_{DT-line}^{inj,max}$, and $S_{DT-line}^{inj,min}$ are reached, then the controller keeps $S_{D-line}^{inj}/S_{DT-line}^{inj}$ at

the saturation limit that has been violated (i.e., same procedure as in Step 3). The stability of the $\tilde{E}$, $\tilde{n}$, and/or $\hat{\gamma}$ cannot be ensured in this case until the controller recovers from the saturation limits. Again, this is not a problem of the control algorithm but just a natural limitation imposed by the available actuation capability. However, in this case, impurity injection is activated for $\tilde{E}$ regulation (Step 5), as long as $n \leq 2 f_{GW} n_{GW}$. If $n > 2 f_{GW} n_{GW}$, impurity injection is never used, as it always increases n. Finally, it can be showed that if $\tilde{E}$, $\tilde{n}$, and $\hat{\gamma}$ are driven to zero with $S_I^{inj} \equiv 0$, then $\tilde{n}_\alpha$ and $\tilde{n}_I$ are also driven to zero as $t \to \infty$ [3], and the control objective is fulfilled.

Step 5: Impurity Injection. By using impurity injection, the controller attempts to drive $n_I \to n_I^*$ such that the $\tilde{E}$ evolution is asymptotically stable. This n_I^* value is obtained by solving the nonlinear equation

$$P_{rad}(n_I^*) = -\frac{\bar{E}}{\tau_E^{min}} + P_\alpha^{min} + P_{Ohm} + P_{aux}^{min} + K_{n_I}\tilde{E}, \tag{27}$$

where $K_{n_I} > 0$ is a design parameter, and P_α^{min} is the α heating achieved by isotopic fueling. Note that $P_{aux} = P_{aux}^{min}$, $\tau_E = \tau_E^{min}$, and $P_\alpha = P_\alpha^{min}$, which means that impurity injection is used only when the combination of auxiliary power modulation (Step 1), in-vessel coil-current modulation (Step 2) and isotopic fueling (Step 3) is not enough to asymptotically stabilize $\tilde{E}$. In this case, (18) reduces to $d\tilde{E}/dt = -\left(1/\tau_E^{min} + K_{n_I}\right)\tilde{E}$. By using $V_{\tilde{E}} = \frac{1}{2}\tilde{E}^2 > 0$ as before, global asymptotical stability of $\tilde{E}$ is ensured because $\dot{V}_{\tilde{E}} = -\left(1/\tau_E^{min} + K_{n_I}\right)\tilde{E}^2 < 0$. It is convenient to define $\hat{n}_I \triangleq n_I - n_I^*$ for stability analysis since making $\hat{n}_I \to 0$ is equivalent to making $n_I \to n_I^*$. By using both this definition and (17), and by taking S_I^{inj} equal to $S_I^{inj,unsat} = \frac{n_I^*}{\tau_I} - S_I^{sp} - K_I\hat{n}_I$, where $K_I > 0$ is a design parameter, it is possible to write $d\hat{n}_I/dt = -(1/\tau_I + K_I)\hat{n}_I$. Taking $V_{\hat{n}_I} = \frac{1}{2}\hat{n}_I^2$, it is found that $\dot{V}_{\hat{n}_I} = -(1/\tau_I + K_I)\hat{n}_I^2 < 0$, which implies $\hat{n}_I \to 0$. Therefore, it can be ensured that $n_I \to n_I^*$ and $\tilde{E} \to 0$. Because of the upper saturation limit that exists for S_I^{inj}, denoted as $S_I^{inj,max}$ (note that $S_I^{inj,min} \equiv 0$), $\tilde{E} \to 0$ cannot be guaranteed until after the controller recovers from saturation.

4.2. Robust Control Law ($\delta_{D-line} \neq 0$, $\delta_{DT-line} \neq 0$)

Step 3: Robust Fueling Rate Modulation ($\tilde{n}_D$ and $\tilde{n}_T$ Control). Equations (15) and (16) can be written in matrix form as $\left[\dot{\tilde{n}}_D, \dot{\tilde{n}}_T\right]^T = f + G\,[u + \delta]$, where $f = \left[-(\bar{n}_D + \tilde{n}_D)/\tau_D + S_D^{inj} - S_\alpha, -(\bar{n}_T + \tilde{n}_T)/\tau_T + S_T^{inj} - S_\alpha\right]^T$,

$$G = \begin{bmatrix} 1-\gamma_{DT-line}^{nom} & 1-\gamma_{D-line}^{nom} \\ \gamma_{DT-line}^{nom} & \gamma_{D-line}^{nom} \end{bmatrix}, \quad u = \begin{bmatrix} S_{DT-line}^{inj} \\ S_{D-line}^{inj} \end{bmatrix}, \quad \delta = G^{-1}\begin{bmatrix} -(\delta_{DT-line}S_{DT-line}^{inj} + \delta_{D-line}S_{D-line}^{inj}) \\ \delta_{DT-line}S_{DT-line}^{inj} + \delta_{D-line}S_{D-line}^{inj} \end{bmatrix}.$$

The nominal control law for $\tilde{n}_D$-$\tilde{n}_T$ is denoted by $\psi_n = [S_{D-line}^{inj}, S_{DT-line}^{inj}]^T$. A control law $u = \psi_n + v$ is now sought, where v is the part to be designed for robustness. Using a similar approach as in [7], v is taken as

$$v = -\frac{\kappa_0\|\psi_n\|_2}{1-\kappa_0}\frac{w}{\|w\|_2} \text{ if } \kappa_0\|\psi_n\|_2\|w\|_2 \geq \epsilon, \quad v = -\left(\frac{\kappa_0\|\psi_n\|_2}{1-\kappa_0}\right)^2\frac{w}{\epsilon} \text{ if } \kappa_0\|\psi_n\|_2\|w\|_2 < \epsilon, \tag{28}$$

where $\epsilon > 0$ is a design parameter that needs to be small, w is given by $w^T = [\frac{\partial V}{\partial \tilde{n}_D}, \frac{\partial V}{\partial \tilde{n}_T}]G$, where $V = V_{\tilde{n}_D} + V_{\tilde{n}_T}$, and κ_0 is a constant that is obtained by finding a bound to δ of the form $\|\delta(\psi_n + v)\|_2 \leq \kappa_0(\|\psi_n\|_2 + \|v\|_2)$. The control law (28) ensures that $|\tilde{n}_D|$ and $|\tilde{n}_T|$ are bounded by class $\mathcal{K}$ functions of ϵ[1]. It can be showed that, provided that $\tilde{E}$ is driven to zero, $|\tilde{n}_\alpha|$ and $|\tilde{n}_I|$ are also bounded by class $\mathcal{K}$ functions of ϵ [3].

Step 4: Robust Fueling Rate Modulation ($\hat{\gamma}$ and $\tilde{n}$ Control). Equations (12) and (13) can be written in matrix form as $\left[\dot{\tilde{n}}, \dot{\hat{\gamma}}\right]^T = f^\star + G^\star[u + \delta^\star]$, where $f^\star = \left[f_1^\star, f_2^\star\right]$, $f_1^\star = 3\left[-\frac{n_\alpha}{\tau_\alpha} + S_\alpha\right] + (3n_\alpha + (1+Z_I)n_I - n)\left(\frac{1-\gamma}{\tau_D} + \frac{\gamma}{\tau_T}\right) - 4S_\alpha + (1+Z_I)\left[-\frac{n_I}{\tau_I} + S_I^{sp}\right]$, $f_2^\star = \gamma(1-\gamma)\left(\frac{1}{\tau_D} - \frac{1}{\tau_T}\right) + \frac{2}{n-3n_\alpha-(1+Z_I)n_I}\{-S_\alpha + 2\gamma S_\alpha\}$, and

$$G^\star = \begin{bmatrix} 2 & 2 \\ 2\frac{\gamma_{DT-line}^{nom}-\gamma}{n-3n_\alpha-(1+Z_I)n_I} & 2\frac{\gamma_{D-line}^{nom}-\gamma}{n-3n_\alpha-(1+Z_I)n_I} \end{bmatrix}, \quad \delta^\star = (G^\star)^{-1}\begin{bmatrix} 0 \\ 2\frac{\delta_{DT-line}S_{DT-line}^{inj}}{n-3n_\alpha-(1+Z_I)n_I} + 2\frac{\delta_{D-line}S_{D-line}^{inj}}{n-3n_\alpha-(1+Z_I)n_I} \end{bmatrix}.$$

The nominal control law for $\hat{\gamma}$-$\tilde{n}$ (isotopic fueling) is denoted by $\psi_n^\star = [S_{D-line}^{inj}, S_{DT-line}^{inj}]^T$. A control law $u = \psi_n^\star + v^\star$ is now sought, where $v^\star$ is the part to be designed for robustness. Following [7], $v^\star$ is taken as

$$v^\star = -\frac{\kappa_0^\star\|\psi_n^\star\|_2}{1-\kappa_0^\star}\frac{w^\star}{\|w^\star\|_2} \text{ if } \kappa_0^\star\|\psi_n^\star\|_2\|w^\star\|_2 \geq \epsilon^\star, \quad v = -\left(\frac{\kappa_0^\star\|\psi_n^\star\|_2}{1-\kappa_0^\star}\right)^2\frac{w^\star}{\epsilon^\star} \text{ if } \kappa_0^\star\|\psi_n^\star\|_2\|w^\star\|_2 < \epsilon^\star, \tag{29}$$

[1] A continuous function $f(x)$ is said to be a class $\mathcal{K}$ function if: (1) it is a strictly increasing function of x, and (2) $f(0) = 0$.

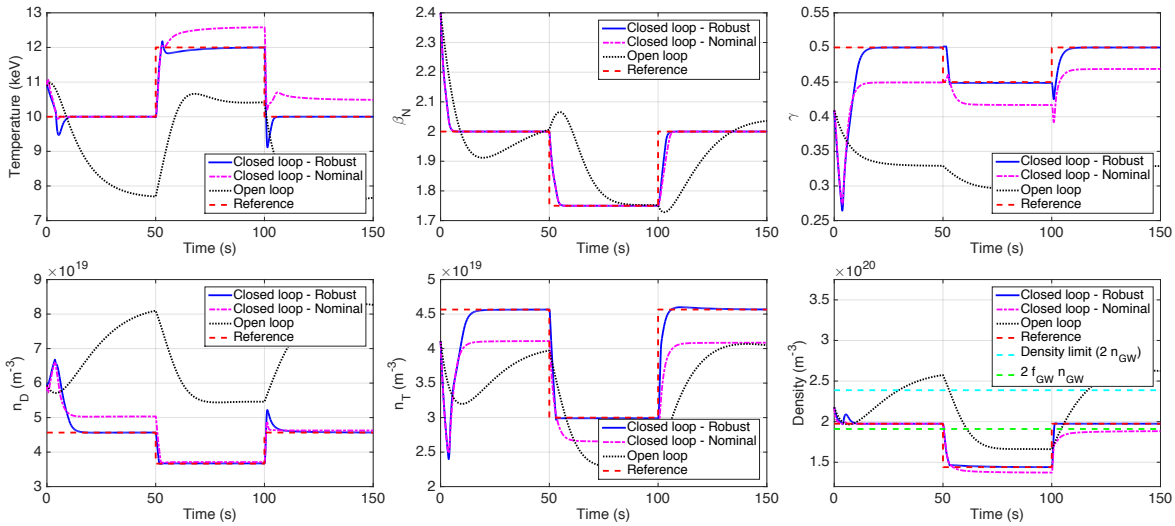

Figure 1: *Time evolutions for T, β_N, γ, n_D, n_T and n under robust feedback control law (solid blue), nominal feedback control law (magenta dashed-dotted), and feedforward control law (black dotted), together with the reference signals (red dashed).*

where $\epsilon^\star > 0$ is a design parameter that needs to be small, $w^\star$ is given by $(w^\star)^T = [\frac{\partial V^\star}{\partial \tilde{n}}, \frac{\partial V^\star}{\partial \tilde{\gamma}}]G^\star$, where $V^\star = V_{\tilde{n}} + V_{\tilde{\gamma}}$, and $\kappa_0^\star$ is a constant that is obtained by finding a bound to $\delta^\star$ of the form $\|\delta^\star(\psi_n^\star + v^\star)\|_2 \leq \kappa_0^\star(\|\psi_n^\star\|_2 + \|v^\star\|_2)$. The control law (29) ensures that $|\tilde{n}|$ and $|\tilde{\gamma}|$ are bounded by class $\mathcal{K}$ functions of $\epsilon^\star$. The proof to show that $|\tilde{n}_\alpha|$ and $|\tilde{n}_I|$ are also bounded by class $\mathcal{K}$ functions of $\epsilon^\star$, provided that $\tilde{E}$ is driven to zero, follows the same arguments as in Step 3. More details can be found in [3].

5. Nonlinear Simulation Study

Simulation results for the evolution of the plasma temperature (T), normalized beta (β_N), tritium fraction (γ), deuterium density (n_D), tritium density (n_T) and total density (n) are showed in Fig. 1. The system inputs are shown in Fig. 2, where the waveforms for S_D^{inj}, S_T^{inj}, S_{D-line}^{inj}, $S_{DT-line}^{inj}$, I_{coil}, and P_{aux} are illustrated. Also, a constant negative 30 % drop in the T concentration of the D-T pellet injector is emulated during the whole simulation, whereas no T is assumed in the D pellet injector (as in the nominal case). Such deviation in the D-T concentration with respect to the nominal case is totally unknown to the controller. Initially, the controller attempts to regulate the system around a first operating point defined by $T = 10$ keV, $\beta_N = 2$, and $\gamma = 0.5$, from $t = 0$ s till $t = 50$ s. The simulation study starts from a perturbed initial condition with respect to this first operating point (+20% in n_α, +30% in n_D, +10% in n_T, and +20% in E (no perturbation is introduced in n_I)). Second, at $t = 50$ s, the controller attempts to drive the system to a different operating point defined by $T = 12$ keV, $\beta_N = 1.75$, and $\gamma = 0.45$. Finally, from $t = 100$ s until $t = 150$ s, the controller attempts to drive the system back to the first operating point. In the case of nominal D-T fuel concentration, the reference actuator signals shown in Fig. 2 are designed to achieve in open loop the desired reference states shown in Fig. 1. However, in presence of the simulated bias in the T concentration of the D-T pellet injector, the variables evolve in open loop to values that are different from the desired references as shown in Fig. 1. Under the nominal control law, β_N is driven to the desired operating points during the whole simulation, whereas T and n can only be driven to the first operating point; at $t = 50$ s, the nominal control law is unable to accurately drive T and n to the second operating point, and it is also unable to drive T and n back to the first operating point at $t = 100$ s. Because $n > 2f_{GW}n_{GW}$ between $t = 0$ s and $t \approx 50$ s, and later between $t \approx 100$ s and $t \approx 150$ s, isotopic fueling is employed, while regular density control is used between $t \approx 50$ s and $t \approx 100$ s. In open loop, n exceeds two times the Greenwald stability limit, while the nominal and robust control laws avoid violating such limit. Still, the nominal control law cannot drive γ, n_D and n_T to the desired operating points during the entire simulation. On the other hand, the robust control law is able to successfully drive all the variables T, β_N, γ, n_D, n_T and n to the different operating points. Fig. 2 shows that the robust control law can correct the drifts in the D-T concentration of the pellet injectors even though they are unknown to the controller, and drives P_{aux}, S_D^{inj}, S_T^{inj} and I_{coil} to their reference values. It must be emphasized that S_{D-line}^{inj} and $S_{DT-line}^{inj}$ are not expected to converge to their reference values due to the emulated bias. The in-vessel coils are utilized by both the nominal and robust control laws during the short periods of time in which P_{aux} is saturated to its minimum value, around $t = 0$ s and $t = 50$ s. Impurity injection is not used at all by the controller due to the fact that, while isotopic fueling is employed, density limits are closed to be violated (i.e., $n > 2f_{GW}n_{GW}$). The simulation study suggests both that the D-T pellet-concentration variations play a crucial role in the burning plasma dynamics and that robust burn controllers are necessary to effectively overcome their negative impact in ITER.

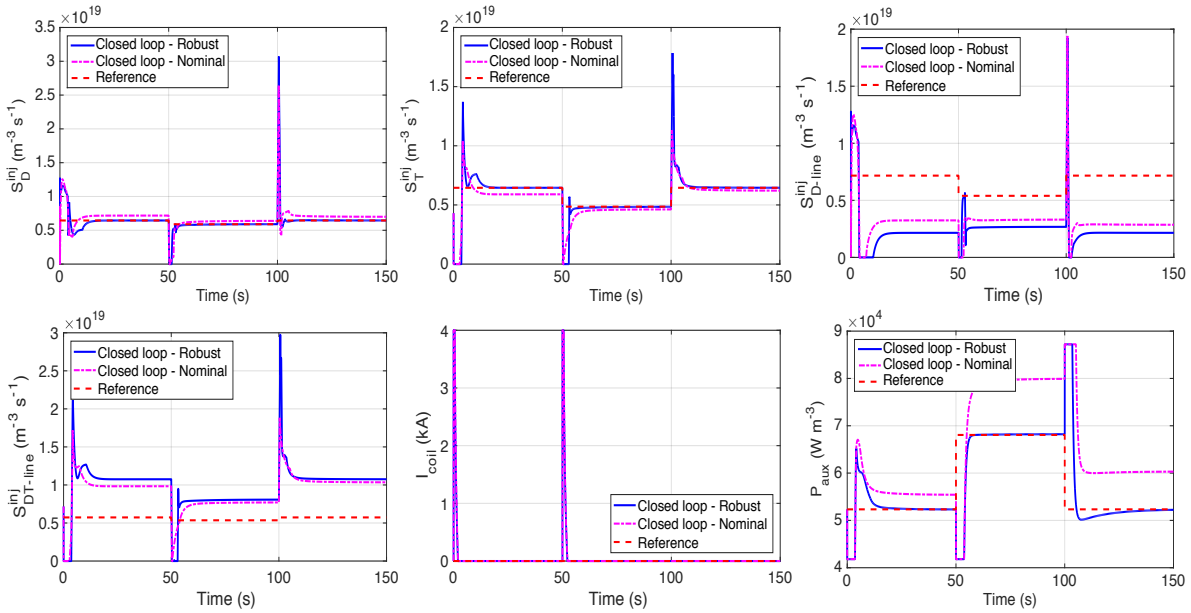

Figure 2: *Actuator signals under robust (solid blue) and nominal (magenta dashed-dotted) control laws, and actuator reference (red dashed).*

6. Conclusions

A nonlinear, robust burn controller, which is capable of regulating the burning plasma system around a desired equilibrium under the presence of large initial perturbations and uncertainties in the DT concentration of the pellet injectors, has been presented. The controller can be used to drive the system between different operating points, since the design process avoids model linearization around a particular equilibrium. Moreover, the algorithm combines all feasible actuators available in tokamaks for burn control (auxiliary power, in-vessel coil current, fueling rates, and impurity injection) in a comprehensive, integrated control strategy, which allows for a high flexibility when choosing the most appropriate actuation methods in different scenarios. For instance, the controller chooses isotopic fueling in scenarios in which disruptive density limits may be reached, whereas it chooses a more accurate D and T density control approach around operating points that are relatively far from disruptive density limits.

Acknowledgments

This work was supported by the US Department of Energy under DE-SC0010661.

Disclaimer

References

[1] R. J. Hawryluk, N. W. Eidietis et al., Control of plasma stored energy for burn control using DIII-D in-vessel coils, Nucl. Fusion, **55** (2015)

[2] L. Hively, Special Topic Convenient Computational Forms For Maxwellian Reactivities, Nucl. Fusion, **17**, 873 (1977)

[3] A. Pajares and E. Schuster, Robust nonlinear burn control in tokamaks to deal with drifts in the fuel-line concentrations, to be submitted to Nuclear Fusion

[4] W. M. Stacey, *Fusion: An Introduction to the Physics and Technology of Magnetic Confinement Fusion*, Wiley-VCH, Weinheim, 2nd edition (2010)

[5] "Summary of the ITER final design report", Technical report, International Atomic Energy Agency, Vienna (2001)

[6] T. E. Evans, Suppression and Mitigation of Edge-Localized Modes in the DIII-D Tokamak with 3D Magnetic Perturbations, Plasma and Fusion Research, **7**, (2012)

[7] H. Khalil, *Nonlinear Systems*, Prentice Hall, 3rd edition (2001)